

Comparison of SuperDARN irregularity drift measurements and *F*-region ion velocities from the resolute bay ISR



Hasan Bahcivan^{a,*}, Michael J. Nicolls^a, Gareth Perry^b

^a Center for Geospace Studies, SRI International, Menlo Park, CA, USA

^b Department of Physics, University of Saskatchewan, Saskatoon, Saskatchewan, Canada

ARTICLE INFO

Article history:

Received 15 March 2012

Received in revised form

10 January 2013

Accepted 5 February 2013

Available online 14 March 2013

Keywords:

RISR

SuperDARN

PolarDARN

ABSTRACT

A number of studies have addressed the principal assumption used by the SuperDARN network of HF radars that the scatter from *F* region field-aligned irregularities has a Doppler shift given by the cosine component of the EXB plasma drift. However, the slopes of the best-fit line to the measured points have consistently been low, perhaps implying contamination from irregularities with smaller amplitude drifts. This work is motivated by testing the same assumption on a more optimal experimental setting: using the north face of the Resolute Bay incoherent scatter radar (RISR-N), which provides high resolution magnitude and direction measurements of EXB drift in a region where the ionospheric flow is mostly uniform relative to auroral latitudes, thereby reducing echo mixing due to spatio-temporal structuring. We compared the EXB drift measured by RISR-N to the line-of-sight Doppler velocities measured PolarDARN which is composed of Rankin Inlet and Inuvik HF radars, both having a field of view over Resolute Bay. An aggregate scatter plot of all the echoes observed during a 5-day period in early May 2011 contains two distinct groups of echoes. The first group is hypothesized to be from the *E* region because the echoes appear above a threshold EXB drift and at small flow angles, which are characteristics of primary Farley–Buneman waves. The Doppler velocity of the second group of echoes increase linearly with the EXB drift and is identified here as *F* region echoes. A special joint fit showed a slope of 0.85 for the *F* region echoes. During the observation period, the *F* region electron density has large variations between 1 and 10×10^{11} , in particular due to the polar cap patches. Considering a representative *F* region electron density of $5 \times 10^{11} \text{ m}^{-3}$, which has a refraction index of 0.86 at 12.5 MHz (for PolarDARN frequencies) and the fact that the measured velocity is the product of the actual velocity and the refractive index, the expected slope is 0.86, in agreement with our measurement. The fit for *E* region Doppler velocities shows a saturation speed at 170 m/s, while the data were spread between 100 and 300 m/s. Although the saturation speed is somewhat lower than the ion acoustic speed, it is acceptable considering earlier work attributing similarly low velocities to large aspect angles at the scattering altitudes.

© 2013 Elsevier Ltd. All rights reserved.

1. Introduction

A variety of plasma waves can be excited in the Earth's high-latitude ionosphere, see Fejer and Kelley (1980) for a comprehensive review of ionospheric irregularities. The strongest *E* region waves are associated with Farley–Buneman instability (Farley, 1963; Buneman, 1963; Hoh, 1963). The waves are generated when the magnitude of the EXB drift exceeds a threshold near the ion acoustic speed. Meanwhile, *F* region small-scale irregularity formation is associated with the gradient drift instability (Reid, 1968; Keskinen and Ossakow, 1982) or the current convective instability (Ossakow and Chaturvedi, 1979;

Chaturvedi and Ossakow, 1979; Vickrey et al., 1980). See Tsunoda (1988) for a review of high-latitude *F* region irregularities. The gradient-drift instability is the most likely source of decameter-scale irregularity generation and it functions through the large Pedersen mobility of the ions as compared to that of electrons. A charge separation is produced when the electric field is directed perpendicular to the plasma density gradient. The resulting polarization electric field will move the plasma with a velocity $\delta \text{EXB}/B^2$ up to the existing gradient which increases further the amplitude of the irregularity. The structure eventually breaks down into smaller ones to decameter scales visible to HF radars.

The SuperDARN network of radars (Greenwald, 1995) is designed to measure these structures to provide wide area coverage of ionospheric circulation. In the case of small turbulent drifts, these structures act as tracers of the plasma drift. Even when $\delta \text{EXB}/B^2$ is large, as long as there is symmetry between density

* Corresponding author. Tel.: +1 650 8594992.

E-mail address: hasan.bahcivan@sri.com (H. Bahcivan).

enhancements and depletions, the mean Doppler shift of the radar echoes will match the cosine component of the EXB drift.

However, the high latitude magnetic geometry poses difficulties in using the Doppler velocities to estimate ionospheric circulation. At most longitudes (except the European sector), it is not possible from the ground to achieve line-of-sight perpendicularity to the magnetic field lines to observe field-aligned irregularities. For the frequency range of 10–20 MHz on which SuperDARN radars operate, perpendicularity is established using refraction (see, for example, Gillies et al., 2009). In the absence of an accurate ionospheric density profile, it may be difficult to ray trace the echoes to their origins in order to identify if the echoes are coming from the *E* or the *F* region. SuperDARN and PolarDARN radars are able to give us elevation angle data, which can be used to identify the origin of the scatter. In most cases, the procedure of separating *E* and *F* region scatters using elevation angle data is straightforward, but for long range gates (> 1000 km), it is harder to separate them. Since the *E* region phase velocities are smaller than those of the *F* region, any injection of *E* region echoes into the receiver would cause an underestimation of the ionospheric circulation speeds.

This work contributes to the previous efforts (Villain et al., 1985; Ruohoniemi et al., 1987; Baker et al., 1990; Davies et al., 1999, 2000; Koustov et al., 2009) on the verification of the FAI drift–EXB correspondence by sorting out *E* and *F* region echoes observed by Rankin Inlet and Inuvik HF radars (together called PolarDARN) and strengthening the basis underlying the *F* region decameter-scale structures as *E* XB tracers. We carefully analyze HF radar Doppler velocities during a period when the north face of the resolute incoherent scatter radar (RISR-N) collected high resolution measurements of the *F* region plasma drift. We inspect time series of ionospheric drift, flow angle, and Doppler velocity from these radars, looking for distinct Doppler characteristics as a function of the EXB drift. Applying a joint fit to the measured *E* and *F* region Doppler velocities, we obtained a slope that is higher and in excellent agreement with the cosine component of the EXB flow (after compensating for the refractive index). We also show that the observed *E* region echo characteristics such as flow angle dependence/drift threshold and slopes are very indicative of primary Farley–Buneman waves.

This paper is organized as follows. First we describe the experiment and discuss RISR-N and PolarDARN data. We then generate a scatter plot of all the data and do a special linear fit. Finally, we conclude with a summary of findings.

2. Experiment description

This experiment covers a 5-day observation period between April 30 and May 4, 2011 during which both RISR-N and PolarDARN collected data continuously. Fig. 1 shows the fields of view PolarDARN and RISR-N. The polygon marks the approximate boundaries of all possible look directions for RISR-N range gates at 300 km-altitude. Only PolarDARN data points that fall in the common observation area (inside the RISR-N polygon) are used for comparison. More precisely, we calculated a representative latitude–longitude “center” of RISR-N ionospheric drift measurements and allowed in PolarDARN data points that are within a maximum of $\pm 2^\circ$ in latitude and $\pm 10^\circ$ in longitude from this center. Additional criteria used to filter out PolarDARN data points are shown in Table 1. In particular, those with low SNR (< 0.5), those with unreasonably high velocity errors (> 500 m/s), and those with small velocity magnitudes were eliminated. The latter two are likely associated with poor fitting of the autocorrelation function and ground clutter. Finally, the time resolution for PolarDARN (RISR-N) is 60 s (90 s). When comparing the two

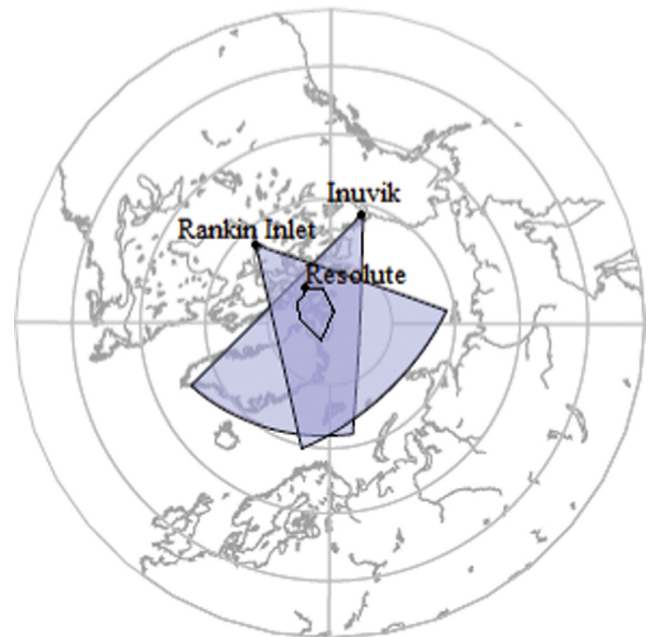


Fig. 1. RISR-N field of view at 300 km altitude (polygon) superimposed on the fields of view for Rankin Inlet and Inuvik radars. Only common area data (within the polygon) are compared.

Table 1
PolarDARN data selection criteria for comparison to RISR-N.

Parameter	Value	Units
Lowest and highest latitude	73.87–77.87	deg.
Lowest and highest longitude	257.44–277.44	deg.
Minimum SNR	0.5	–
Minimum velocity	100	m/s
Maximum vel. error	500	m/s

Table 2
Resolute North radar parameters.

Parameter	Value	Units
Frequency	441.9	MHz
Peak power	1.8	MW
Duty cycle	10.0	%
HPFB	1.0	deg.
IPP	10	ms
Range resolution	72	km
Altitude range	0–743	km
Time resolution	90	s
Magnetic dip angle	86.45–88.38	deg.
Geographic latitude	74.72955 N	deg.
Geographic longitude	–94.90576 E	deg.
Magnetic latitude	82.77 N	deg.
Magnetic longitude	323.18 E	deg.
Magnetic local time	UT-7	hours
Solar local time	UT-6	hours

datasets, we associated a PolarDARN data point with a RISR-N one if the time separation is < 45 s.

Table 2 shows the system parameters of RISR-N for this experiment; see Bahcivan et al. (2010) for additional information on RISR-N such as the beam configuration. A total of 11 radar beams were used to illuminate the ionosphere, however, only three of the beams that provided the highest Doppler velocity accuracy were used. Note that the accuracy depends on the

signal-to-noise ratio, the number of samples, and the particular ACF lags used. We obtained mean ion drifts by least-squares fitting a uniform horizontal flow velocity vector to the observed line-of-sight velocities measured between the altitudes of 200 and 400 km. We looked for a pair of perpendicular electric fields and an ion velocity component parallel to \mathbf{B} that best fits the second and third lags of the autocorrelation functions. The key is to minimize statistical fluctuations by averaging over altitude ranges for which ACF lags maintain the same sign. For instance, we cannot do this over the fourth lag because depending on the electron/ion temperatures, the ACF may change sign. The second author fits each ACF from a particular range and beam according to the incoherent scatter theory using the free parameters N_e , T_e , T_i , and V_i and uses all the V_i measurements to come up with an electric field. Note that the velocity estimation methods were derived independently by the first and the second authors and the results agreed well. Furthermore, the third author independently compared a segment of RISR-N data with Rankin line-of-sight measurements and validated the derived technique by the first author.

3. Observations

Fig. 2 shows the entire time series of RISR-N measurements projected along the respective lines-of-sights of Rankin Inlet and Inuvik radars (black lines) and Doppler velocity (red circles) measured by these radars (top panel for Rankin Inlet and the bottom panel is for Inuvik radar). Note that the velocities are positive when echo is moving away from the radar. We mainly observe two groups of echoes: (1) those with small velocity magnitudes (200–300 m/s) and (2) those that follow the EXB cosine component very closely. The low velocity echoes occur when the line-of-sight velocity (in general the EXB magnitude) is above a threshold. Note that the sign of the low velocity echoes matches the sign of the EXB cosine component. Hereinafter, we refer to the first (second) group of points as E (F) region echoes. Next, we select the four 8-h long segments and analyze echo occurrence in terms of EXB flow angle with respect to the PolarDARN line-of-sight.

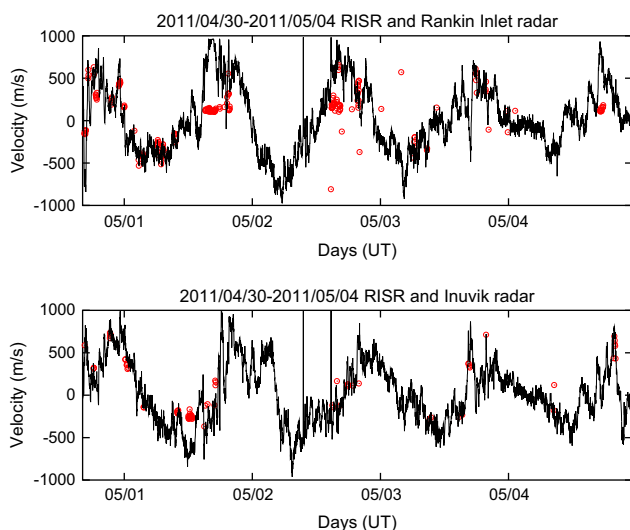


Fig. 2. F region ion drift velocities (measured by RISR-N) projected along the PolarDARN radars' lines-of-sight (positive means moving away). The red dots mark the PolarDARN measured Doppler velocities. The top and bottom panels are for Rankin Inlet and Inuvik radars, respectively. (For interpretation of the references to color in this figure caption, the reader is referred to the web version of this article.)

Fig. 3 shows two of those periods. The blue line is the flow angles (0° —looking directly into the flow, 90° —perpendicular to the flow, 180° —opposite to the flow). The black line and the red circles are the same as in Fig. 2. The first echoes in the top left panel (for Rankin Inlet) occurred at ~ 1630 when the line-of-sight speed decreased below ~ -600 m/s (EXB drift magnitude increased to > 900 m/s). The Doppler velocities for these echoes were near -200 m/s (negative velocity means the target is moving away). The flow angle was $\sim 135^\circ$ (EXB drift is away from the radar). The next set of echoes occurred at 1715 and 1815 UT when the flow angles were $15\text{--}20^\circ$ and the EXB magnitude was ~ 600 m/s. But these have Doppler velocities precisely matching the EXB cosine component. The fourth set of echoes occurred when the drift had the same flow angle range but somewhat larger EXB magnitude (~ 750 m/s) and the Doppler velocities were ~ 300 m/s, much less than the EXB cosine component (~ 650 m/s). A similar pattern occurred on the upper-right (Rankin Inlet): the Doppler velocity of the first two groups of echoes matched well with the EXB cosine component during which EXB magnitude was below ~ 500 m/s, while later a much larger set of echoes occurred with Doppler velocities of ~ 150 m/s when the EXB magnitude was > 700 m/s and the flow angles were small ($10\text{--}45^\circ$). This pattern is also valid for Inuvik radar (lower two panels), although there are cases (such as 2120 UT, lower left panel) where the measured Doppler velocities matched EXB cosine component even though the flow was around 700 m/s and the flow angles were small $< 20^\circ$.

The same pattern can be seen in Fig. 4 where we show the time series for the next two selected periods. In particular, in the upper-left panel we see the alternation of E and F region echoes between 1500 and 1700 UT and in the upper-right panel the sudden appearance of E region echoes, all occurring when the flow angle is small and the EXB magnitude is large. Fig. 5 is a scatter plot of PolarDARN Doppler velocities vs. the cosine component of EXB projection velocity measured by RISR-N. The scatter plot is for data collected over 4–5 days. It can be seen that the points are concentrated into two regions: (1) those that are concentrated around 200 m/s and (2) those that follow a linear line with a slope close to unity. The blue and red lines which are together defined by two parameters (slope and offset) are best fits (in terms of minimum distance) to the entire dataset including both radars and both E and F regions. The slope of the blue line is 0.85 and the offset of the red lines is 170 m/s. Note that the Doppler velocity of F region echoes is presumed to follow a slope of 1 (assuming refractive index is unity), while E region echoes have smaller Doppler velocities, near the ion acoustic speed (Bahcivan et al., 2005). Although the saturation speed (~ 170 m/s) indicated by the first group of echoes (following the red line) is somewhat lower than C_s , we will refer to them as E region echoes, in consideration of the previous work (Makarevich et al., 2006, 2007; Gorin et al., 2012) also reporting similarly low velocities at HF.

4. Discussion

We ran a ray racing model for two sets of ionospheric parameters to determine if there can be overlap between E and F region echoes for the ranges where we compared RISR-N and SuperDARN velocities. Fig. 6 shows the ray traces of HF beams at 12 MHz. The traces are separated by 1° elevation angle increments. Yellow segments mark where the backscatter perpendicularity (to the geomagnetic field) condition is met, that is, where we expect backscatter. The ionospheric parameters are shown at the top. The RISR–PolarDARN comparison were made using data from the range 1400 to 1850 km. In the top panel, we can see that

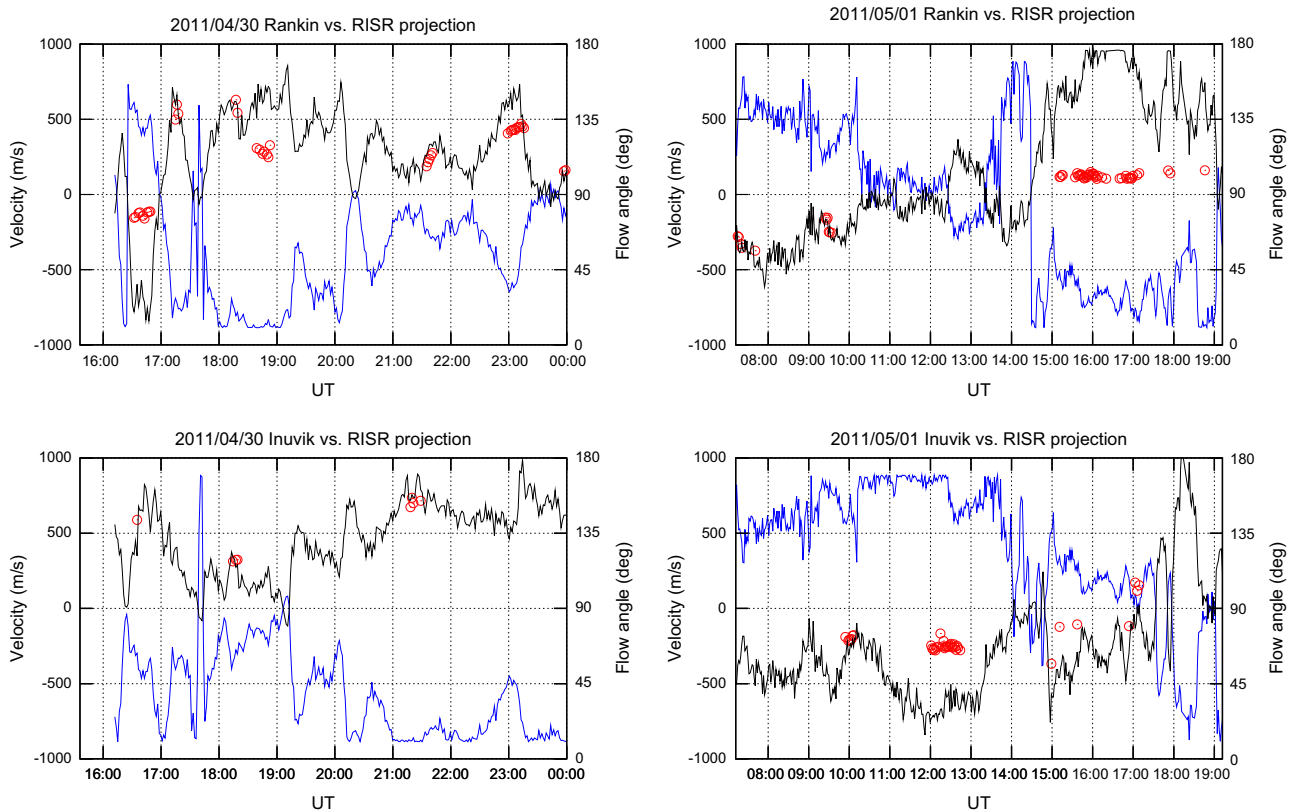


Fig. 3. PolarDARN measured Doppler velocities (red dots), RISR-N measured *F* region ion velocity projected on PolarDARN lines-of-sight (black line), and the *F* region ion flow angle with respect to the PolarDARN lines-of-sight (blue line). Shown are the two time periods on April 30 and May 1 in 2011 (left and right columns). The top and bottom panels are for Rankin Inlet and Inuvik radars, respectively. (For interpretation of the references to color in this figure caption, the reader is referred to the web version of this article.)

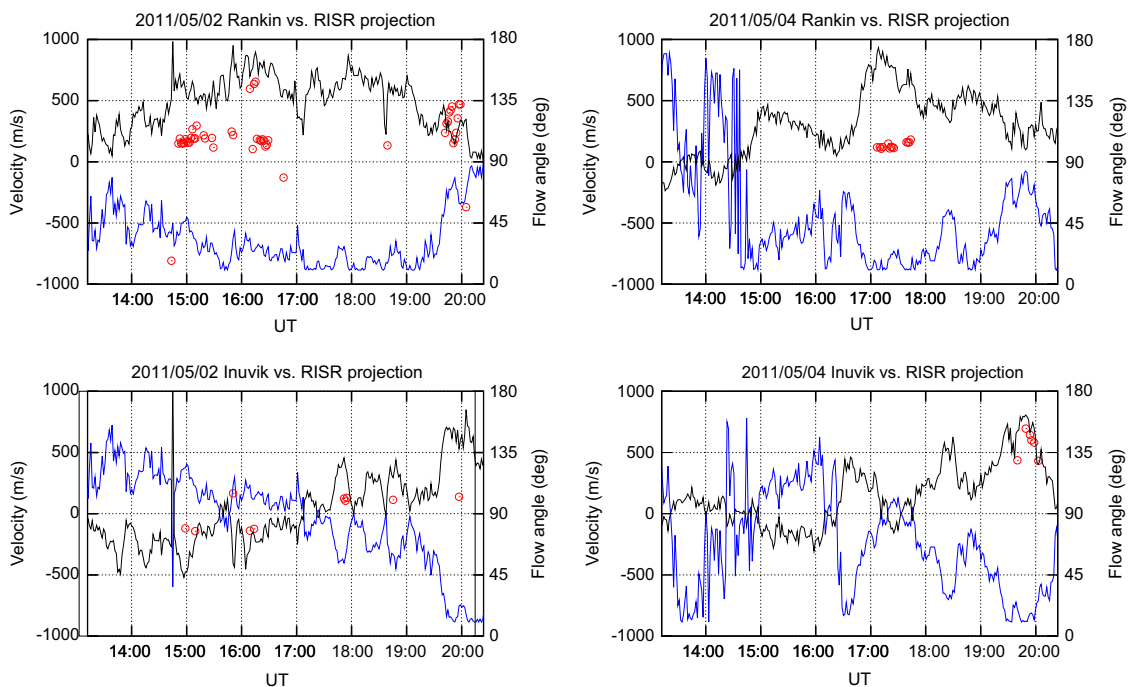


Fig. 4. Same as Fig. 3 but for another two periods on May 2 and 4 in 2011 (left and right columns).

this range contains points of perpendicularity between the altitudes of 200 and 300 km. Echoes from *E* region altitudes occur near the ranges of 1200 km. The bottom panel shows ray tracing results for larger electron densities which result in greater

refraction and more complicated scattering geometry. In this case, we see that the perpendicularity condition is met between the ranges 500–1000 km and 2000–2500 km but not in the ranges where we made the RISR–PolarDARN comparison. Therefore, the

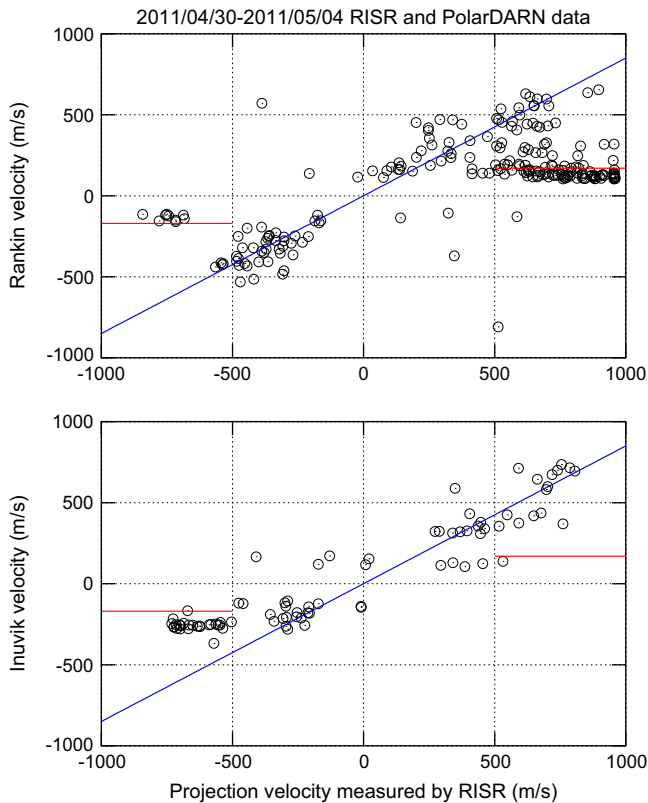


Fig. 5. Scatter plots of Doppler velocity of PolarDARN radars vs. the F region ion velocity projected along the lines-of-sight. Top and bottom panels for Rankin Inlet and Inuvik radars, respectively. The blue and red line fits are together defined by two parameters (slope and offset). (For interpretation of the references to color in this figure caption, the reader is referred to the web version of this article.)

ray racing model shows that E and F region echoes may arrive from various ranges, depending on the ionospheric density profile. Moreover, the ray tracing model assumes an isotropic ionosphere between the radar and scattering regions, which may not necessarily be true. We therefore expect significant variability in the backscatter location for long ranges and it is difficult to conclusively sort out E and F region echoes based on arrival angle. Nevertheless, E region echoes at these long ranges have been seen before (Lacroix and Moorcroft, 2001; Milan et al., 1997) and this strengthens our hypothesis that PolarDARN radars are able to see E region echoes.

We now visit the previous work on the propagation speed of F region irregularities. One of the earliest works on this topic is that of Ruohoniemi et al. (1987) who compared Sondrestrom ion drifts to HF radar. They found a slope of 1.4, after manually removing some of the data points most inconsistently with the least squares fit of the data. This is the only paper so far that showed HF velocity larger than EXB drift. One can see from a comparison of Figures 10 and 11 in their papers that some of those removed points occurred for large ion drifts exceeding about 600 m/s, suggesting that another instability process is being excited at large plasma drifts, perhaps involving the Farley–Buneman instability in the E region. Another study is by Baker et al. (1990) who compared drift measurements using DMSP-F9 satellite to irregularity drift velocity measurements from the HF coherent radar sited at Halley Bay in Antarctica. There were only 7 data points matching well with the EXB drift assumption, although only 2 points were for plasma drifts above 600 m/s. Moreover, Villain et al. (1985) compared HF Doppler spectra to EISCAT ion drifts. The mean spectral shifts were shown to closely (within 45°) match the cosine component of the EXB flow. More

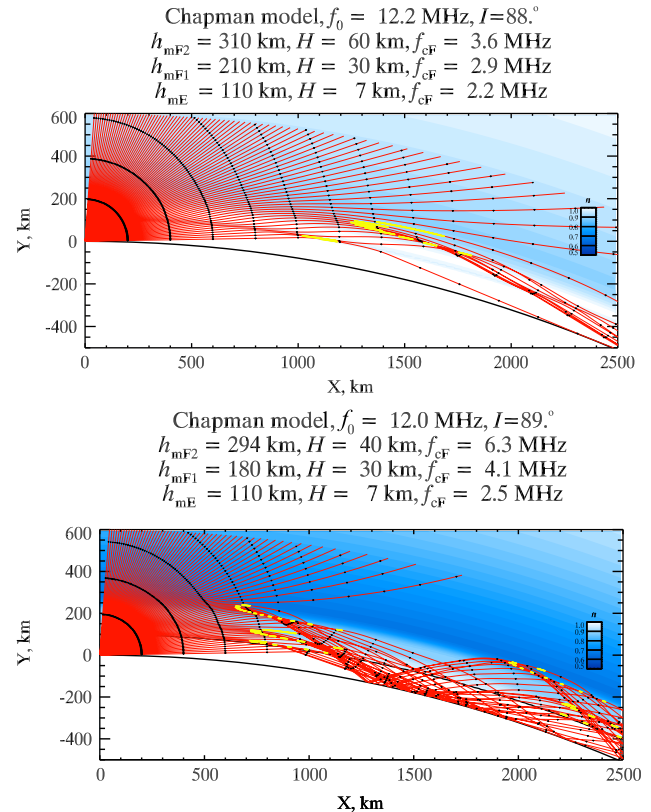


Fig. 6. Ray traces of HF beams (red), shown at 1° elevation angle increments for two sets of ionospheric parameters (top and bottom panels). Yellow segments mark the locations where the HF beam is within 1° of perpendicularity to the magnetic field. (For interpretation of the references to color in this figure caption, the reader is referred to the web version of this article.)

interesting to us was the actual projection of the cosine component on the spectral shape itself (see their Figure 10). The spectra generally composed of multiple peaks and, in almost every spectral example shown, the EXB cosine component was coinciding with one of the distinct peaks. We consider this work as a clear evidence of the EXB drift–FAI motion equivalence, although the tendency in this work and later ones is to consider the mean Doppler shift alone as a quantity describing the ion drift, which often provides poorer correspondence.

Xu et al. (2001) were the first ones who clearly stated that the SuperDARN F region velocities are below EXB. The data came from an observational geometry similar to what is considered in this manuscript. In particular they reported the effect of stronger HF velocity underestimation at larger EXB velocities. Meanwhile, Davies et al. (1999) compared 4 h of CUTLASS Finland HF radar velocities with the projected F region ion velocity measured by the EISCAT UHF system. Although the HF velocities follow well the cosine component of EXB for flows smaller than several hundred km/s, for larger velocities the discrepancy grew significantly (in line with the result from Xu et al., 2001). Combination of all the data points yielded a slope of 0.73. Davies et al. (1999) attributed some of the discrepancies to contamination by E region echoes as the CUTLASS–EISCAT distance is not sufficiently large to guarantee that any scatter observed over EISCAT will be from the F region. In a subsequent study, Davies et al. (2000) compared a much larger set of measurements collected over 4 days from the CUTLASS Finland HF radar with the EISCAT Svalbard and VHF radars. Davies et al. (2000) concluded “remarkable” agreement between HF irregularity drift measurements and the ISR measurements, without a least-squares-fit to determine the slope. A closer inspection of the Figure 3 in their work shows significantly

large data spread and data asymmetries, which may have been caused by the mixing of *E* region echoes into the observations. Furthermore, there are not significant data points beyond ~ 600 m/s (the threshold over which we expect *E* region echoes to show up) and those beyond are far from the hypothetical slope of 1.

Some of the more recent comparison of HF radar to ISRs have lead to only an approximate or partial confirmation of the FAI drift-EXB equivalence. Koustov et al. (2009) compared Rankin Inlet radar velocities with measurements from the HF radar in Saskatoon, the CADI ionosonde at Resolute Bay, and drift meters on board DMSP satellites passing through the Rankin Inlet radar field of view. Koustov et al. (2009) found that the slope of the best fit line for Rankin Inlet velocities as a function of the cosine component of the EXB plasma drift is 0.7 or lower. In particular, in about half of the cases, it was found that Rankin Inlet measurements underestimate DMSP velocity projections by a factor of 2 or less. A closer inspection of Figure 4 in Koustov et al. (2009) (Rankin Inlet-DMSP comparison) shows a significant concentration of events with Rankin Inlet velocities between negative 200 and 300 m/s, similar to the concentration of data points we found in this velocity range (see the top panel of Fig. 5) and associated with *E* region scatter. It is therefore possible that the mixing of lower velocity *E* echoes into the statistics caused the slope reported by Koustov et al. (2009) to be lower. Most recently, Gillies et al. (2010) compared EISCAT and Finland SuperDARN measurements. Despite trying various estimates of N_e in the scattering volume, the velocities measured by SuperDARN were still lower. Gillies et al. (2010) hypothesized that this is because of dense N_e structures which significantly reduce the refractive index to account for the low Doppler velocities. Our findings here do not support to refute this hypothesis, however, we find it important to point out the asymmetry in their Figure 1, which is a scatter plot of Doppler velocities similar to Figure 5 of this paper. The asymmetry is near 200 m/s for EISCAT velocities of 400–500 m/s and, although not certain, we suspect that this asymmetric feature is caused by *E* region echoes.

5. Conclusion

A number of studies have addressed the principal assumption used by the SuperDARN network of HF radars that the scatter from *F* region field-aligned irregularities has a Doppler shift given by the cosine component of the EXB plasma drift. However, the slopes of the best-fit line to the measured points have consistently been low, implying Doppler velocities of smaller amplitudes. In this work, we tested the same assumption on a more optimal experimental setting using the Resolute Bay incoherent scatter radar providing accurate and high resolution velocity and angular resolution measurements of EXB drift and in a polar region where the ionospheric flow is mostly uniform relative to lower latitudes, thereby reducing echo mixing due to spatio-temporal structuring. We compared the EXB drift measured by RISR-N to PolarDARN (composed of Rankin Inlet and Inuvik radars with a field of view that includes Resolute Bay) and have the following findings:

1. The scatter plots of the PolarDARN radar Doppler velocities vs. the cosine component of the EXB drift contain two distinct regions: one region with smaller velocities and occurring above a certain EXB threshold (see the third finding below) and the other region obeying the EXB velocity (*F* region). Although we have not established with certainty that the first region is due to *E* region backscatter, we hypothesize here that

it is so because of the saturated velocities, thresholding, and flow angle dependence that are the characteristics of Farley-Buneman waves observed in the *E* region.

2. The *F* region Doppler velocities are given by the cosine component of the EXB drift. In this study, we measure the slope as 0.85. We have looked at RISR-N N_e estimates for the altitudes of 200–350 km in May 1, 2011 and observed a variation between 10^{11} m³ (no polar cap patches) and 10^{12} m³ (patches). Considering a middle value (5×10^{11} m³) electron density, yielding a refraction index of 0.86 at 12.5 MHz (for PolarDARN frequencies), and the fact that $\mathbf{v}_{measured} = \mathbf{v}_{real} \cdot \mathbf{n}$ (Ginzburg, 1970), the expected slope corresponding to EXB drifting irregularities should have been 0.86, in agreement with what we measured. However note that ionospheric electron density has significant diurnal variations and will significantly change when polar cap patches are present.
3. The *E* region echoes are excited when (i) the magnitude of the EXB drift exceeds a threshold of ~ 600 m/s and (ii) the flow angle is small, between 0° and 45° or 135° and 180° . This finding is in line with the previous studies reporting that echoes are much stronger in the main flow direction (Bahcivan et al., 2005; Kelley et al., 2008). This suggests that it is the primary Farley-Buneman waves dominating the received backscatter during small flow angles.
4. The fit for *E* region echoes shows a saturation at 170 m/s. Although somewhat lower than the ion acoustic speed, it is acceptable considering the previous work (Makarevich et al., 2006, 2007; Gorin et al., 2012) also reporting similarly low velocities at HF, attributed to the decrease in velocity at large aspect angles.
5. The implication of this work for SuperDARN measurements is that if EXB drift is greater than ~ 600 m/s, *E* region echoes with lower velocities are likely to mix into observations. Due to the large dynamic range of coherent scatter (> 60 dB), we anticipate that the autocorrelation function shape will be dominated by scatter from either of the regions (it is possible that the ACFs composed of comparable scatter from each region will be marked as poor fit and removed). If not removed or compensated, ionospheric circulation will be underestimated by these radars.

Acknowledgments

This work was completed under the NSF cooperative agreement ATM-0608577 to SRI International.

References

- Bahcivan, H., Hysell, D.L., Larsen, M.F., Pfaff, R.F., 2005. The 30 MHz imaging radar observations of auroral irregularities during the JOULE campaign. *Journal of Geophysical Research* 110, A05307, <http://dx.doi.org/10.1029/2004JA010975>.
- Bahcivan, H., Tsunoda, R., Nicolls, M., Heinselman, C., 2010. Initial ionospheric observations made by the new resolute incoherent scatter radar and comparison to solar wind IMF. *Geophysical Research Letters* 37, L15103, <http://dx.doi.org/10.1029/2010GL043632>.
- Baker, K.B., Greenwald, R.A., Ruohoniemi, J., Dudeney, J.R., Pinnock, M., Newell, P.T., Greenspan, M.E., Meng, C.I., 1990. Simultaneous HF-radar and DMSP observations of the cusp. *Geophysical Research Letters* 17 (11), 1869–1872.
- Buneman, O., 1963. Excitation of field aligned sound waves by electron streams. *Physical Review Letters* 10, 285–287.
- Chaturvedi, P.K., Ossakow, S.L., 1979. Nonlinear stabilization of the $\mathbf{E} \times \mathbf{B}$ gradient drift instability in ionospheric plasma clouds. *Journal of Geophysical Research* 84, 419.
- Davies, J.A., Lester, M., Milan, S.E., Yeoman, T.K., 1999. A comparison of velocity measurements from the CUTLASS Finland radar and the EISCAT UHF system. *Annals of Geophysics* 17, 892–902.
- Davies, J.A., Yeoman, T.K., Lester, M., Milan, S.E., 2000. Letter to the editor: a comparison of F-region ion velocity observations from the EISCAT Svalbard and VHF radars with irregularity drift velocity measurements from the CUTLASS Finland HF radar. *Annals of Geophysics* 18, 589–594.

- Farley, D.T., 1963. A plasma instability resulting in field-aligned irregularities in the ionosphere. *Journal of Geophysical Research* 68, 6083.
- Fejer, B.G., Kelley, M.C., 1980. Ionospheric irregularities. *Reviews of Geophysics* 18, 401.
- Gillies, R.G., Hussey, G.C., Sofko, G.J., McWilliams, K.A., Fiori, R.A.D., Ponomarenko, P., Maurice, J.-P.St., 2009. Improvement of SuperDARN velocity measurements by estimating the index of refraction in the scattering region using interferometry. *Journal of Geophysical Research* 114, A07305, <http://dx.doi.org/10.1029/2008JA013967>.
- Gillies, R.G., Hussey, G.C., Sofko, G.J., Wright, D.M., Davies, J.A., 2010. A comparison of EISCAT and SuperDARN F-region measurements with consideration of the refractive index in the scattering volume. *Journal of Geophysical Research* 115, A06319, <http://dx.doi.org/10.1029/2009JA014694>.
- Ginzburg, V.L., 1970. *The Propagation of Electromagnetic Waves in Plasmas*. Pergamon, Oxford, UK.
- Gorin, J.D., Koustov, A.V., Makarevich, R.A., Maurice, J.-P.St., Nozawa, S., 2012. Velocity of E-region HF echoes under strongly-driven electrojet conditions. *Annals of Geophysics* 30, 235–250.
- Greenwald, R.A., 1995. SuperDARN: a global view of high-latitude convection. *Space Science* 71, 763.
- Hoh, F.C., 1963. Instability of Penning-type discharge. *Physics of Fluids* 6, 1184.
- Kelley, M.C., Cuevas, R.A., Hysell, D.L., 2008. Radar scatter from equatorial electrojet waves: an explanation for the constancy of the Type I Doppler shift with zenith angle. *Geophysical Research Letter* 35, L04106, <http://dx.doi.org/10.1029/2007GL032848>.
- Keskinen, M.J., Ossakow, S.L., 1983. Theories of high-latitude ionospheric irregularities: a review. *Radio Science* 18, 1093.
- Koustov, A.V., Maurice, J.-P.St., Sofko, G.J., Andre, D., MacDougall, J.W., Hairston, M.R., Fiori, R.A., Kadochnikov, E.E., 2009. Three-way validation of the Rankin Inlet PolarDARN radar velocity measurements. *Radio Science* 44, <http://dx.doi.org/10.1029/2008RS004045>.
- Lacroix, P.J., Moorcroft, D.R., 2001. Ion acoustic HF radar echoes at high latitudes and far ranges. *Journal of Geophysical Research* 106 A12, 29091–29103.
- Makarevich, R.A., Senior, A., Koustov, A.V., Uspensky, M.V., Honary, F., Dyson, P.L., 2006. A study of aspect angle effects in the E-region irregularity velocity using multi-point electric field measurements. *Geophysical Research Letters* 33, L21102, <http://dx.doi.org/10.1029/2006GL027740>.
- Makarevich, R.A., Koustov, A.V., Senior, A., Uspensky, M.V., Honary, F., Dyson, P.L., 2007. Aspect angle dependence of the E-region irregularity velocity at large flow angles. *Journal of Geophysical Research* 112, A11303, <http://dx.doi.org/10.1029/2007JA012342>.
- Milan, S.E., Yeoman, T.K., Lester, M., Thomas, E.C., Jones, T.B., 1997. Initial backscatter occurrence statistics from the CUTLASS HF radars. *Annals of Geophysics* 15, 703–718.
- Ossakow, S.L., Chaturvedi, P.K., 1979. Current convective instability in the diffuse aurora. *Geophysical Research Letters* 86, 332.
- Reid, G.G., 1968. The formation of small-scale irregularities in the ionosphere. *Journal of Geophysical Research* 73, 1627.
- Ruohoniemi, J.M., Greenwald, R.A., Baker, K.B., Villain, J.P., 1987. Drift motions of small-scale irregularities in the high-latitude F region: an experimental comparison with plasma drift motions. *Journal of Geophysical Research* 92 (A5), 4553–4564.
- Tsunoda, R.T., 1988. High latitude F region irregularities: a review and synthesis. *Reviews of Geophysics* 87, 9171.
- Vickrey, J.F., Rino, C.L., Potemra, T.A., 1980. Chatanika/triad observations of unstable ionization enhancements in the auroral F region. *Geophysical Research Letters* 7, 789.
- Villain, J.P., Caudal, G., Hanuise, C., 1985. A SAFARI-EISCAT comparison between the velocity of F region small-scale irregularities and the ion drift. *Journal of Geophysical Research* 90 (A9), 8433–8443.
- Xu, L., Koustov, A.V., Thayer, J., McCready, M., 2001. SuperDARN convection and Sondrestrom plasma drift. *Annals of Geophysics* 19, 749–759.